Chinese Chemical Letters 33 (2022) 4605–4609

Contents lists available at ScienceDirect

Chinese Chemical Letters

journal homepage: www.elsevier.com/locate/cclet

A hybrid nano-assembly with synergistically promoting photothermal and catalytic radical activity for antibacterial therapy

Yunxia Wang[a], Chuangxin Zhang[a], Hui Zhang[a], Liheng Feng[a,*], Libing Liu[b,c,*]

[a] School of Chemistry and Chemical Engineering, Shanxi University, Taiyuan 030006, China
[b] Department of Nutrition and Health, China Agricultural University, Beijing 100193, China
[c] Beijing National Laboratory for Molecular Sciences, Institute of Chemistry, Chinese Academy of Sciences, Beijing 100190, China

ARTICLE INFO

Article history:
Received 2 December 2021
Revised 10 March 2022
Accepted 16 March 2022
Available online 19 March 2022

Keywords:
Conjugated oligomer
Nano-assembly
Fenton reaction
Photothermal therapy
Bacterial infections

ABSTRACT

It is of great significance to develop effective antibacterial agents and methods to combat drug resistant bacterial infections due to its increasing threaten to human health and the ineffectiveness of antibiotics. Herein, a multifunctional hybrid nano-assembly (M1-Fe NPs) based on conjugated oligomer and ferrous ion was engineered with favorable bactericidal activity for synergetic antibacterial therapy. The chelation of ferrous ion not only enhances the photothermal conversion efficiency of M1 but also endows the nano-assembly with catalytic capability of transferring H_2O_2 into stronger oxidant hydroxyl radicals (•OH). Meanwhile, the generated heat can further promote the Fenton reaction activity. By generating cytotoxic heat and oxidative •OH, M1-Fe NPs can effectively kill Staphylococcus aureus in vitro and in vivo with the aid of low dosage of H_2O_2. The work provides a new multifunctional platform for combinational drug resistant antibacterial therapy and even antitumor therapy.

Although the generation of various antibiotics, the drug resistant bacterial infections still threaten the health of human being over the world [1–4]. It is emergent to develop effective antibacterial agents and antibacterial strategies to resist the evolution of bacteria and eliminate the damage from bacterial infections. By now, different kinds of materials have been developed to antibacterial agents relied on diverse antibacterial mechanisms [5–10]. Ag-based materials can kill bacteria by inhibiting replication through the binding of Ag ions with ATP synthetic enzymes [11]. Cationic polymers, quaternary ammonium salts, and antibacterial peptides can perturb and disrupt the cell membrane of bacteria to induce the death of bacteria [12–15]. Conjugated polymer [16–20], metal-organic frameworks [21–23], black phosphorus [24,25], copper sulfide [26,27], Au- [28–30] and carbon-based materials [31,32] can generate reactive oxygen species (ROS) or heat under light irradiation to oxidize or damage phospholipids, proteins and even DNA to kill bacteria, which is involved in photodynamic therapy (PDT) and photothermal therapy (PTT). In addition, hydrogels are also developed as multifunctional anti-infective materials by combining above mentioned antibacterial mechanism with ability of tissue repair [33]. However, there are still some disadvantages in current antibacterial agents for practical antibacterial therapy, such as low antibacterial ability and long-term cytotoxicity, and it remains a challenge to develop highly effective antibacterial agents and strategies with low biological toxicity and little possibility to trigger drug resistance.

PDT and PTT are considered to be effective antibacterial therapies with characteristics of broad-spectrum antibacterial activity, spatial and temporal control and low side effects [34]. The ROS and hyperthermia generated by photosensitizers and photothermal agents can kill all type of bacteria, including antibiotic resistant strains, with little chance to induce drug resistance. However, these two therapies have respective shortcomings, such as the limited damage to bacteria due to the oxygen-dependent antibacterial activity and the unnecessary damage to normal cells due to the excessive ROS and temperature [35,36]. To address the issues, combined therapy of PDT and PTT is increasingly developed to maximize the advantages of two therapies and make up for the shortages of each other. Hydroxyl radical (•OH) is one kind of ROS and has stronger oxidation ability than other ROS, such as H_2O_2 and $^1O_2$ [37,38]. Moreover, •OH can be generated by decomposition of H_2O_2 with the aid of ferrous ion (Fe^{2+}), which termed as Fenton reaction [39], without dependence of oxygen. It shows remarkable advantage over oxygen-dependent traditional PDT. Hence, Fenton reaction has attracted broad interest of researchers for development of chemodynamic therapy (CDT). Increasing works focus

* Corresponding authors.
E-mail addresses: lhfeng@sxu.edu.cn (L. Feng), liulibing@iccas.ac.cn (L. Liu).

https://doi.org/10.1016/j.cclet.2022.03.076
1001-8417/

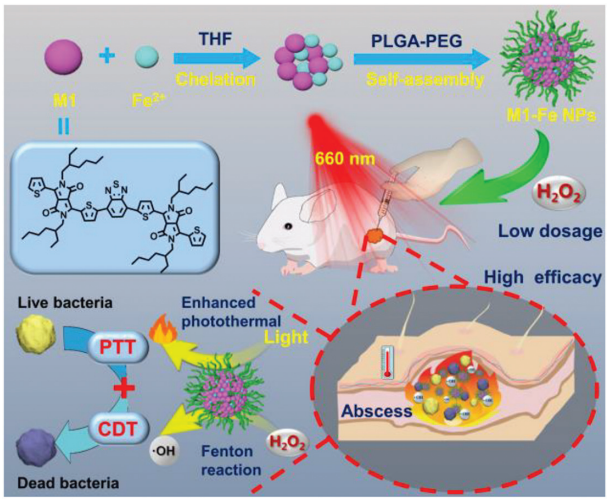

Scheme 1. Schematic illustration of designed multifunctional hybrid nano-assembly M1-Fe NPs for highly effective and synergetic antibacterial therapy.

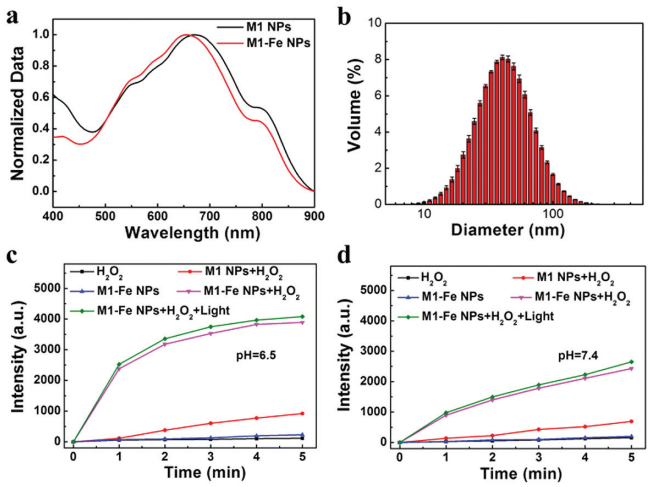

Fig. 1. (a) Normalized UV-vis absorption spectra of M1 NPs and M1-Fe NPs. (b) DLS distribution of M1-Fe NPs. Average size is 59.7 ± 0.5. (c) Detection of produced ·OH by different groups at pH 6.5 and (d) 7.4.

on the selection of nanomaterials and strategy to enhance the efficiency of CDT, offering important findings and rational instructions to the development of antitumor therapy [39,40]. As most CDT agents are inorganic materials, organic materials also begin to be applied. Although the combined PTT and CDT for cancer treatment has been intensively investigated, for the antibacterial therapy combined two therapies remains rare, especially that mediated by organic materials. Therefore, it is imperative to develop organic materials with photothermal and catalytic Fenton reaction activity to realize synergistic treatment of bacterial infections.

In this work, to effectively eradicate bacteria and lower the damage to normal tissue, we proposed a new antibacterial strategy of photothermal and chemodynamic synergistic promotion. Accordingly, we developed a hybrid nano-assembly with photothermal and catalytic Fenton reaction activity for synergetic antibacterial therapy (Scheme 1). The nano-assembly, termed as M1-Fe NPs, is comprised of ferrous ion-chelated conjugated oligomer M1 and amphiphilic polymer PLGA-PEG. M1 is designed to chelate with Fe^{2+} offering catalytic activity of Fenton reaction and also act as photothermal agent. Furthermore, the chelation with Fe^{2+} can in turn enhance the photothermal effect of M1. Hence, in the presence of H_2O_2 and light irradiation (660 nm), M1-Fe NPs can catalyze decomposition of H_2O_2 to generate stronger oxidizer ·OH to damage bacteria. Meanwhile, the heat generated by M1 can further kill bacteria and promote the generation of ·OH by accelerating Fenton reaction. Taking *Staphylococcus aureus* (*S. aureus*) as a typical representative, the synergistic damage of heat and ·OH can effectively kill it by destroying membrane, proteins, enzyme and DNA. Besides, under light irradiation, M1-Fe NPs successfully treat *S. aureus*-infected wound of mice at the aid of low dosage of H_2O_2. Therefore, this work provides a hybrid nano-assembly based on conjugated oligmer to achieve highly effective and synergistic antibacterial PTT and CDT, and it also offers a novel multi- functional antibacterial platform for effective anti-infective therapy.

Conjugated oligomer M1 is a kind of photothemal agent and can be prepared to nanoparticle M1-NPs, which has been reported by our previous literature [41]. Its synthetic route is shown as Fig. S1 (Supporting information). However, it is necessary to develop new method to improve the photothmal property for better antibacterial application. Since the molecular structure of M1 contains heteroatoms such as sulfur and nitrogen, it is promise to have good chelation between M1 and Fe^{2+}. The chelation probably changes the molecular configuration and light absorption ability of M1. And Fe^{2+} is considered to have catalytic Fenton reaction activity that is heat-related and benefits antibacterial application. Therefore, Fe^{2+} is designed to chelate with M1 to change the photothermal property and endow M1 with catalytic activity of Fenton reaction at the same time for obtaining enhanced antibacterial capability.

M1 was cheated with Fe^{2+} and then mixed with PLGA-PEG to prepare nanoparticles noted as M1-Fe NPs by nanoprecipitation method. The optical properties of chelated compound (M1-Fe) and nanoparticles were next investigated. As shown in Fig. S2 (Supporting information), the maximum absorption peak of oligomer M1 had an obvious blue-shift from 642 nm to 610 nm after chelated with Fe^{2+}. Even processed to nanoparticles, the obvious blue-shift from 670 nm to 655 nm in the absorption spectra was still found (Fig. 1a). It indicates that the chelation between M1 and Fe^{2+} exist and is stable. Besides, the formation of nanoparticles made absorption spectrum broader (extending to 900 nm), especially better absorption at 660 nm, which provided excellent conditions for photothermal therapy. At an excitation wavelength of 650 nm, almost no fluorescence peak was observed in the fluorescent spectrum (ranging from 700 nm to 900 nm) of M1-Fe NPs (Fig. S3 in Supporting information), which further facilitated the conversion from light to heat. The average hydrodynamic diameter of M1-Fe NPs was measured to be ~60 nm by using dynamic light scattering (DLS) and was shown in Fig. 1b. To further understand the morphology of M1-Fe NPs, scanning electron microscopy (SEM) was employed. As shown in Fig. S4 (Supporting information), M1-Fe NPs showed a uniformly spherical shape.

Next, to verify the catalytic activity of M1-Fe NPs for catalyzing decomposition of H_2O_2, aminophenylfluorescein (APF) was used to detected the production of ·OH by measuring the fluorescence of oxidized APF [42]. Considering the acidic microenvironment at the site of infection, the detection was performed at a pH of 6.5. As shown in Fig. 1c, compared with M1 NPs, M1-Fe NPs can catalyze H_2O_2 to generate more ·OH with stronger fluorescent intensity. After light irradiation, the amount of generated ·OH was a little more, which might because M1-Fe NPs generate heat to accelerate the heat-related catalytic reaction. With the pH at 7.4, the generated ·OH was obviously lower than that of 6.5 (Fig. 1d). It indicates the introduction of Fe^{2+} endows the nanoparticles with catalytic property and the catalytic activity is potential to be better in bacterial microenvironment under light irradiation.

The ability of converting light to heat is important for photothermal antibacterial application, therefore, we investigated the

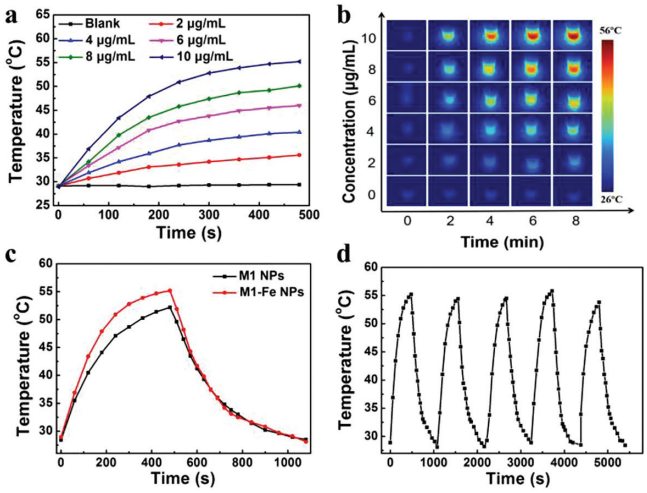

Fig. 2. (a) Temperature changes and (b) infrared thermal images of M1-Fe NPs with different concentrations under light irradiation (660 nm, 1.0 W/cm^2). (c) Temperature profiles of M1 NPs and M1-Fe NPs under the same experimental condition (660 nm, 1.0 W/cm^2), respectively. (d) Temperature curve of M1-Fe NPs for 5 cycles of on/off light irradiation (660 nm laser, 1 W/cm^2).

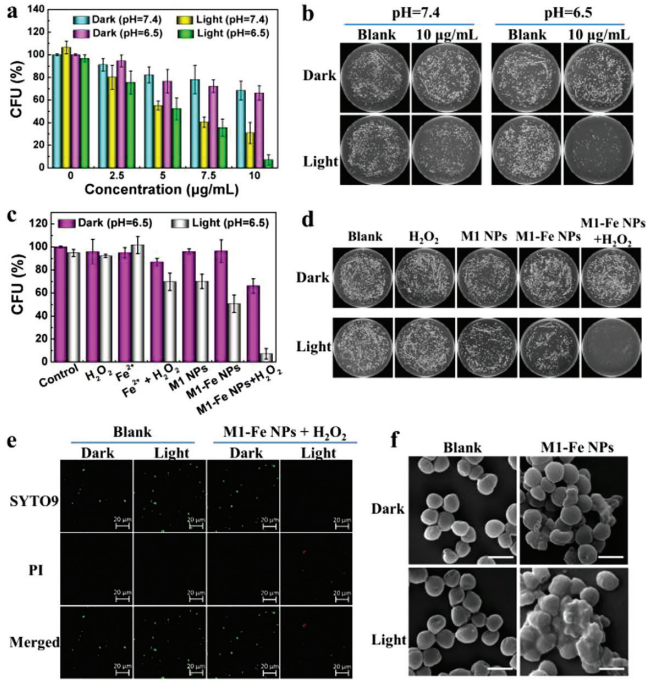

Fig. 3. (a) Antibacterial activity of M1-Fe NPs with the aid of H_2O_2 under different concentration and pH conditions. (b) Corresponding bacterial plate images at killing concentration (10.0 μg/mL). (c) Antibacterial activity of different components at pH of 6.5 in dark or under irradiation and corresponding (d) bacterial plate images. (e) Fluorescence staining and (f) SEM images of *S. aureus* without and with treatment of M1-Fe NPs + H_2O_2 in dark or under irradiation. The scale bars are 20 μm in (e) and 1 μm in (f). Data are presented as mean ± SD ($n = 3$). The light is a 660 nm laser (1.0 W/cm^2). The concentration of M1-Fe NPs is 10.0 μg/mL. The concentration of H_2O_2 is 1 mmol/L.

photothermal property of M1-Fe NPs, and a 660 nm laser was used to irradiate nanoparticle solution. At a power density of 1.0 W/cm^2, the temperature of M1-Fe NPs dispersion with different concentrations increased to varying degrees and the increase was positively correlated with nanoparticles concentrations and irradiation time (Fig. 2a). After an irradiation of 8 min, the temperature of M1-Fe NPs was up to to 55 °C at a low concentration of 10.0 μg/mL, which indicated M1-Fe NPs had good photothermal capability. The corresponding thermal images that visualized the temperature changes of solutions are displayed as Fig. 2b. In addition, the increase of temperature was also positively correlated with power density of light. As shown in Fig. S5 (Supporting information), the temperature of M1-Fe NPs (10.0 μg/mL) increased to 60 °C at an irradiated power density of 1.25 W/cm^2. To further verify the boost effect of Fe^{2+} on the photothermal property of M1 NPs, we compared the temperature changes of two nanoparticles under the same condition. As shown in Fig. 2c, the temperature of M1-Fe NPs was higher than that of M1 NPs about 4 °C. It proved that the chelation indeed enhanced the photothermal conversion capability of M1 NPs. After five heating-cooling cycles, the temperature profiles of M1-Fe NPs were little changed, indicating the good photothermal stability (Fig. 2d). All above mentioned results illustrate that fabricated M1-Fe NPs are potential to be applied in the photothermal antibacterial application.

After verifying the photothermal and catalytic property of M1-Fe NPs, we next examined its antibacterial activity against planktonic bacteria. *S. aureus* is chosen as the model bacteria for it is a common pathogen and has better heat resistance [43]. H_2O_2 is employed as a source of •OH. Considering that the microenvironment of bacterial infected site was acidic, we performed the antibacterial experiment at a pH of 6.5 to simulate the infected environment, and set pH of 7.4 as contrast condition. As shown in Fig. 3a, bacterial viability was decreased with the increase of M1-Fe NPs concentration, proving efficient and synergistic dual treatment mode. The corresponding bacterial plates are displayed as Fig. 3b and Fig. S6 (Supporting information). In contrast, even treated with the highest concentration of M1-Fe NPs, about 70% of bacteria were still alive at pH of 7.4 and 6.5 without light irradiation. It indicates that •OH generated by decomposition of H_2O_2 is not enough to eradicate bacteria. As the light introduced, the bacterial activity decreased obviously, no matter pH was 7.4 or 6.5. It verifies that heat plays an important role in killing bacteria. The decrease of bacterial activity was more remarkable at pH of 6.5, stating that the Fenton reaction was favored by the heat and acidic condition. These results illustrate that M1-Fe NPs are potential to effectively kill bacteria at infected site by generating heat and catalyzing H_2O_2.

To figure out the synergistic antibacterial effect of heat and •OH, *S. aureus* was treated with H_2O_2, Fe^{2+}, $H_2O_2 + Fe^{2+}$, M1 NPs, M1-Fe NPs, and M1-Fe NPs + H_2O_2, respectively. The concentration of M1-Fe NPs is 10.0 μg/mL. As shown in Fig. 3c, under light irradiation, the •OH generated from catalytic decomposition of 1 mmol/L H_2O_2 by individual Fe^{2+} could only kill 30% of bacteria. The heat generated from M1-Fe NPs under the same light irradiation damaged 50% of bacteria. Without light irradiation, the •OH generated from catalytic decomposition of H_2O_2 by M1-Fe NPs might inhibit 34% of bacteria. In contrast, 95% of bacteria could be killed by M1-Fe NPs and H_2O_2 under the same light irradiation. The corresponding bacterial plates are displayed in Fig. 3d and Fig. S7 (Supporting information). The result proves that the heat and •OH synergistically kill bacteria to obtain the best antibacterial effect in M1-Fe NPs-mediated antibacterial therapy.

Further, the antibacterial mechanism of M1-Fe NPs with aid of H_2O_2 was investigated. After different treatments, *S. aureus* was stained by SYTO9 and PI to observe the state of bacteria through confocal laser scanning microscopy (CLSM). As shown in Fig. 3e, bacteria treated with M1-Fe NPs and H_2O_2 without light irradiation was mostly stained by SYTO9 showing green fluorescence. It indicates that most bacteria have intact membrane and kept alive. While, the bacteria was almost all stained by PI showing red fluorescence when light was performed. It demonstrates that the membranes of bacteria are ruptured and bacteria are dead. To further observe the morphology of bacteria after different treatments,

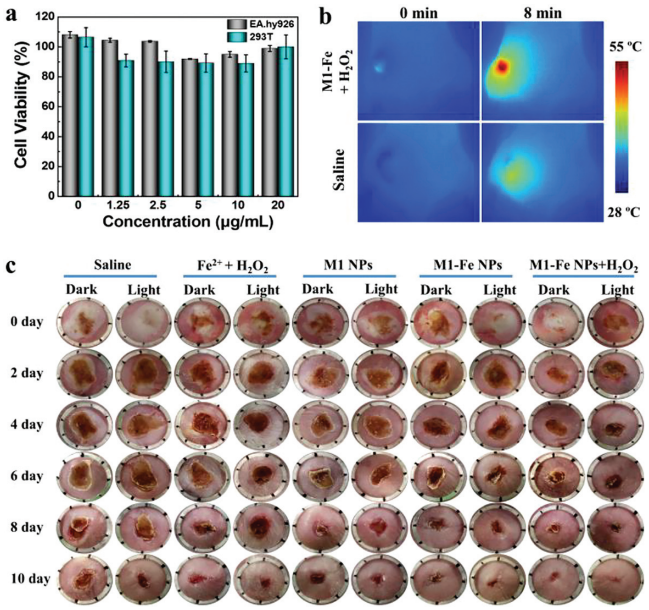

Fig. 4. (a) Cell viability of EA.hy926 and 293T after treatment of M1-Fe NPs with different concentrations. (b) Infrared thermal images of infected wound of mice after different treatments (660 nm, 1.0 W/cm^2). (c) Photographs of *S. aureus*-infected wounds of mice after 10-day treatment by various therapies.

SEM was employed to capture the images of bacteria. As depicted in Fig. S8 (Supporting information), the surface of bacteria treated with Fe^{2+} and H_2O_2 had a little collapsed, which might result from the oxidative damage of •OH that generated by Fe^{2+}-catalyzed decomposition of H_2O_2. For bacteria treated with M1 NPs and M1-Fe NPs without light irradiation had little morphology change compared to that of blank group. However, upon light irradiation, the surface of some bacteria was fused, which might result from the heat produced by nanoparticles. Only the bacteria treated with M1-Fe NPs and H_2O_2 under light irradiation appeared obvious wrinkled and fused morphology (Fig. 3f). It indicates that the heat and •OH generated by M1-Fe NPs and H_2O_2 synergistically break the membrane structure and other components of bacteria to kill them.

After understanding the antibacterial effects of M1-Fe NPs and H_2O_2, we next investigated their anti-infective ability. Firstly, the cytotoxicity of M1-Fe NPs was determined by standard MTT method. As shown in Fig. 4a, M1-Fe NPs had little effect on the growth of two human cells EA.hy926 and 293T even at a concentration of 20.0 μg/mL, implying the low cytotoxicity and application possibility of M1-Fe NPs for anti-infective treatment. Then *S. aureus*-infected mice modes were established to perform the anti-infective experiment. All animal procedures were performed according to the relevant laws and guidelines approved by the Animal Care and Use Committee of Shanxi University. Besides the treatment of M1-Fe NPs + H_2O_2, other treatments including saline, H_2O_2 + Fe^{2+}, M1 NPs, and M1-Fe NPs were performed as control treatments. The concentration of H_2O_2 was 1.0 mmol/L, a low concentration for antibacterial application [38,44]. Each treatment involved two groups: dark and light. The light group employed a 660 nm laser and the power density was 1.0 W/cm^2 plus an irradiation time of 8 min. As displayed in Fig. 4b, after laser irradiation, the temperature of wound treated with M1-Fe NPs + H_2O_2 increased to 55 °C, which was obviously higher than that of saline treated (43 °C). Such locally high temperature of 55 °C can kill most bacteria and trigger little damage to normal tissue. Hence, the wound area of mice in M1-Fe NPs + H_2O_2 plus light group decreases about 60% on the fourth day, which decreased the most in all groups (Fig. S9 in Supporting information). And after a 10-day treatment, the wound treated with M1-Fe NPs + H_2O_2 under light irradiation had the best healing effect compared to other treatments (Fig. 4c). It confirms that the synergistic PTT/CDT based on M1-Fe NPs and H_2O_2 can effectively treat *S. aureus*-infected wound and get the best therapeutic effect than any other single therapy. All of the results demonstrated that M1-Fe NPs-mediated synergistic antibacterial therapy had a great potential for highly effective and safe treatment of bacterial infection.

In summary, we have fabricated a multifunctional hybrid nanoassembly (M1-Fe NPs) based on conjugated oligomer M1 and Fe^{2+} for synergetic PTT/CDT antibacterial therapy. The introduction of Fe^{2+} not only increased the photothermal conversion property (increased 4 °C at 10.0 μg/mL), but also endowed the nanoparticles with catalytic capability of transferring H_2O_2 into stronger oxidant •OH. Moreover, the generated heat could further accelerate the catalytic decomposition of H_2O_2 to kill more bacteria. Hence, upon light irradiation, the M1-Fe NPs could efficiently kill *S. aureus* with the aid of low dosage H_2O_2, which antibacterial effect was better than any other monotherapy. Finally, they also treated the *S. aureus*-infected wound of mice. This study offers a novel drug resistant antibacterial platform for effective, safe and synergistic anti-infective therapy.

Declaration of competing interest

The authors report no declarations of interest.

Acknowledgments

We are grateful to the National Natural Science Foundation of China (Nos. 21977065, 22177065 and 21807067), SanJin Scholars Support Plan under Special Funding (No. 2017-06), Scientific and Technological Innovation Programs of Higher Education Institutions in Shanxi (Nos. 201802106, 2019L0022), Supported by the Fund for Shanxi "1331" Project (1331), and the Program for Introducing Overseas High-level Talents of Shanxi (Hundred Talents Plan).

Supplementary materials

Supplementary material associated with this article can be found, in the online version, at doi:10.1016/j.cclet.2022.03.076.

References

[1] J.M.V. Makabenta, A. Nabawy, C.H. Li, et al., Nat. Rev. Microbiol. 19 (2021) 23–36.
[2] S. Sarva, J.S. Harinath, S.P. Sthanikam, et al., Chin. Chem. Lett. 27 (2016) 16–20.
[3] H.J. Zhang, Y.C. Liang, H. Zhao, et al., Macromol. Biosci. 20 (2020) 1900301.
[4] Z.L. Li, W. Lu, S.C. Jia, et al., ACS Appl. Bio. Mater. 4 (2021) 370–386.
[5] Z.L. Li, H.T. Bai, S.C. Jia, et al., Mater. Chem. Front. 5 (2021) 1236–1252.
[6] S.Q. Li, S.J. Dong, W.G. Xu, et al., Adv. Sci. 5 (2018) 1700527.
[7] T.J. Dai, C.P. Wang, Y.Q. Wang, et al., ACS Appl. Mater. Interfaces 10 (2018) 15163–15173.
[8] Y. Fu, L. Yang, J.H. Zhang, et al., Mater. Horiz. 8 (2021) 1618–1633.
[9] L.Q. Mei, S. Zhu, Y.P. Liu, et al., Chem. Eng. J. 418 (2021) 129431.
[10] C. Hu, Y.J. Yang, Y.Q. Lin, et al., Adv. Drug Deliv. Rev. 178 (2021) 113967.
[11] H. Kong, J. Jang, Langmuir 24 (2008) 2051–2056.
[12] P. Li, Y.F. Poon, W. Li, et al., Nat. Mater. 10 (2011) 149–156.
[13] D.F. He, Y.F. Tan, P.F. Li, et al., Chin. Chem. Lett. 32 (2021) 1743–1746.
[14] S. Yan, S. Chen, X. Gou, et al., Adv. Funct. Mater. 29 (2019) 1904683.
[15] M.M. Zhu, Y. Fang, Y.C. Chen, et al., J. Colloid Interface Sci. 584 (2021) 225–235.
[16] Q.F. Cui, H.B. Yuan, X.Y. Bao, et al., ACS Appl. Bio. Mater. 3 (2020) 4436–4443.
[17] C. Zhang, K.G. Wang, X.Y. Guo, Y.L. Tang, J. Mater. Chem. C 10 (2022) 2600–2607.
[18] T.T. Zhou, R. Hu, L.R. Wang, et al., Angew. Chem. Int. Ed. 59 (2020) 9952–9956.
[19] M.M. Hou, Y.X. Zhong, L. Zhang, et al., Chin. Chem. Lett. 32 (2021) 1055–1060.
[20] L.Y. Zhou, F.T. Lv, L.B. Liu, et al., CCS Chem. 1 (2019) 97–105.
[21] J.H. Liu, D. Wu, N. Zhu, Y.N. Wu, G.L. Li, Trends Food Sci. Technol. 109 (2021) 413–434.
[22] D. Mao, F. Hu, Kenry, et al., Adv. Mater. 30 (2018) 1706831.
[23] W. Teng, Z.J. Zhang, Y.K. Wang, et al., Small 17 (2021) 2102315.
[24] C.Y. Mao, Y.M. Xiang, X.M. Liu, et al., ACS Nano 12 (2018) 1747–1759.

[25] L.F. Wang, Y. Li, L. Zhao, et al., Nanoscale 12 (2020) 19516–19535.
[26] Y. Qiao, Y. Ping, H.B. Zhang, et al., ACS Appl. Mater. Interfaces 11 (2019) 3809–3822.
[27] Y.N. Li, N. Li, J. Ge, et al., Biomaterials 201 (2019) 68–76.
[28] C. Liu, M. Zhang, H.Q. Geng, et al., Appl. Catal. B 295 (2021) 120317.
[29] Y.K. Zheng, H. Jiang, X.M. Wang, Chin. Chem. Lett. 31 (2020) 3183–3189.
[30] M. Zhang, H.R. Zhang, J. Feng, Y.L. Zhou, B.L. Wang, Chem. Eng. J. 393 (2020) 124778.
[31] Q. Xin, H. Shah, A. Nawaz, et al., Adv. Mater. 31 (2019) 1804838.
[32] A. Anand, B. Unnikrishnan, S.C. Wei, et al., Nanoscale Horiz. 4 (2019) 117–137.
[33] G. Gao, Y.W. Jiang, H.R. Jia, F.G. Wu, Biomaterials 188 (2019) 83–95.
[34] Z.J. Cheng, T. Zhang, W.L. Wang, et al., Chin. Chem. Lett. 32 (2021) 1580–1585.
[35] K. Zhang, X. Meng, Y. Cao, et al., Adv. Funct. Mater. 28 (2018) 1804634.
[36] R. Wu, H.Z. Wang, L. Hai, et al., Chin. Chem. Lett. 31 (2020) 189–192.
[37] P. Hu, T. Wu, W.P. Fan, et al., Biomaterials 141 (2017) 86–95.
[38] J.Q. Xi, G. Wei, Q.W. Wu, et al., Biomater. Sci. 7 (2019) 4131.
[39] Z.M. Tang, Y.Y. Liu, M He, W.B. Bu, Angew. Chem. Int. Ed. 58 (2019) 946–956.
[40] S.S. He, Y.Y. Jiang, J.C. Li, K.Y. Pu, Angew. Chem. Int. Ed. 59 (2020) 10633–10638.
[41] H. Zhang, L.X. Guo, Y.X. Wang, et al., Biomater. Sci. 9 (2021) 2137–2145.
[42] K.Y. Ni, G.X. Lan, S.S. Veroneau1, et al., Nat. Commun. 9 (2018) 4321.
[43] S.R. Zhou, Z.J. Wang, Y.X. Wang, L.H. Feng, ACS Appl. Bio Mater. 3 (2020) 1730–1737.
[44] Y.N. Liu, Z.R. Guo, F. Li, et al., ACS Appl. Mater. Interfaces 11 (2019) 31649–31660.